

# S<sup>3</sup>CE-Net: Spike-guided Spatiotemporal Semantic Coupling and Expansion Network for Long Sequence Event Re-Identification

Xianheng Ma   Hongchen Tan   Xiuping Liu   Yi Zhang   Huasheng Wang   Jiang Liu  
Ying Chen   Hantao Liu

## Abstract

In this paper, we leverage the advantages of event cameras to resist harsh lighting conditions, reduce background interference, achieve high time resolution, and protect facial information to study the long-sequence event-based person re-identification (Re-ID) task. To this end, we propose a simple and efficient long-sequence event Re-ID model, namely the Spike-guided Spatiotemporal Semantic Coupling and Expansion Network (S<sup>3</sup>CE-Net). To better handle asynchronous event data, we build S<sup>3</sup>CE-Net based on spiking neural networks (SNNs). The S<sup>3</sup>CE-Net incorporates the Spike-guided Spatial-temporal Attention Mechanism (SSAM) and the Spatiotemporal Feature Sampling Strategy (STFS). The SSAM is designed to carry out semantic interaction and association in both spatial and temporal dimensions, leveraging the capabilities of SNNs. The STFS involves sampling spatial feature subsequences and temporal feature subsequences from the spatiotemporal dimensions, driving the Re-ID model to perceive broader and more robust effective semantics. Notably, the STFS introduces no additional parameters and is only utilized during the training stage. Therefore, S<sup>3</sup>CE-Net is a low-parameter and high-efficiency model for long-sequence event-based person Re-ID. Extensive experiments have verified that our S<sup>3</sup>CE-Net achieves outstanding performance on many mainstream long-sequence event-based person Re-ID datasets. **Code is available at:** <https://github.com/Mhsunshine/SC3E-Net>.

## 1. Introduction

Video-based person re-identification (Re-ID) aims to retrieve a specific person among numerous input video sequences [8]. Current methods [7, 21, 41, 59, 65, 72] primarily rely on RGB data and design various spatiotemporal feature extraction modules to effectively address challenges in Re-ID tasks, such as viewpoint changes, occlusion, and pose variations. However, traditional RGB cameras struggle to perceive effective person semantics under conditions of high exposure or low lighting. Some excellent work has

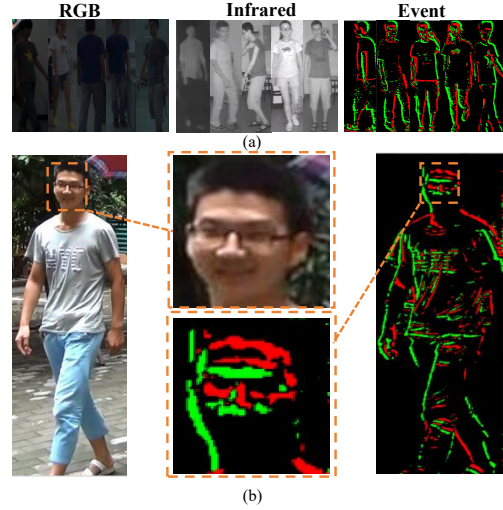


Figure 1. (a) Display of person information in RGB, Infrared, and Event modalities under low-light conditions. (b) Display of facial detail comparison in RGB and Event modalities.

studied Re-ID under infrared modality [66, 67]. Although these methods have achieved excellent results, both types of cameras face a common challenge: persons are easily distracted by background information, motion blur, and the exposure of their facial information.

Recently, event cameras [16] have emerged as a promising sensor technology, capable of recording pixel-level brightness changes. As shown in Fig.1-(a), compared to RGB/Infrared cameras, event cameras exhibit not only resistance to extreme lighting conditions but also significantly reduce interference from background information [38, 56]. Furthermore, as illustrated in Fig.1-(b), event cameras offer an advantage over RGB cameras by minimizing the leakage of personal portrait information. Additionally, the high temporal resolution of event cameras ensures that motion blur is not easily induced in the event modality. Given these advantages of the event modality, there is considerable potential for developing high-quality Re-ID models.

Despite these advantages, the event modality also presents unique challenges. First, the spatial sparsity of

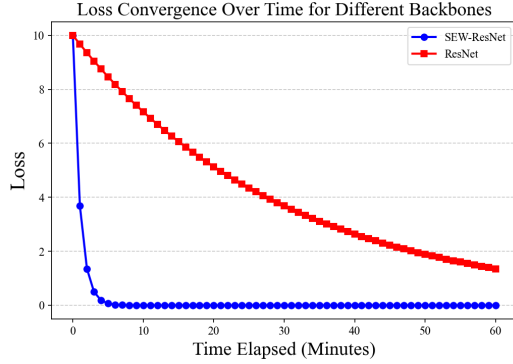


Figure 2. Convergence of the SNNs’ Backbone (depicted by the blue line, SEW-ResNet) and the CNNs’ Backbone (depicted by the red line, ResNet).

event streams necessitates the association of events across different time points in order to obtain meaningful spatial features. Additionally, the high temporal resolution of event cameras generates a large volume of event data, necessitating the development of efficient processing methods to extract useful information while avoiding excessive computational complexity.

Current mainstream video-based Re-ID methods are predominantly based on Deep Convolutional Networks (DCNs) [7, 21, 59, 72]. However, DCNs face significant limitations when handling event camera data, particularly in efficiently processing sparse and asynchronous event streams. Furthermore, DCNs are often associated with high energy consumption and latency, rendering them unsuitable for resource-constrained or real-time applications. Recent Transformer-based approaches [22, 46] attempt to achieve simultaneous interaction of temporal and spatial semantics, but they require significant computational overhead. In contrast, Spiking Neural Networks (SNNs) [44], inspired by biological neural networks, transmit information through discrete spikes and only perform computations when input events are received. This design enables SNNs to achieve low latency and low power consumption, making them especially well-suited for asynchronous event streams. Accordingly, the asynchronous nature of SNNs aligns perfectly with the characteristics of event streams [47], allowing them to effectively process sparse and high temporal resolution inputs while activating and accumulating temporal semantics. As shown in Fig. 2, in the Re-ID task based on event data, SNNs’ Backbone (depicted by the blue line, SEW-ResNet) converges faster than CNNs’ Backbone (depicted by the red line, ResNet). However, SNNs also face difficulties in achieving spatiotemporal correlation interactions between discrete and sparse semantics, which is not conducive to representation of compact person descriptors.

Besides, we know that current deep models often con-

centrate on a small subset of key semantics while overlooking other valid semantics. For event modalities with extremely sparse semantics, the “lazy” nature of deep models can easily render person descriptors less robust. A series of neural models adopt the feature dropout strategy [20, 51, 55, 77] in an attempt to improve the robustness of the model. Additionally, BCP [54] extracts strip-shaped patch features to perceive and capture effective semantics. However, due to the extreme sparsity of event semantics, the dropout strategy often falls into empty areas with a high probability, and the semantic information contained within the strip-shaped regions may be too limited to meet the recognition requirements.

To solve the above two issues, we propose a simple and efficient long-sequence event Re-ID model, the Spike-guided Spatiotemporal Semantic Coupling and Expansion Network ( $S^3$ CE-Net). To better perceive and accumulate key semantics efficiently from sparse and asynchronous event streams, we adopt the Spike element-wise ResNet (SEW-ResNet) [14] to build our  $S^3$ CE-Net. The  $S^3$ CE-Net contains the Spike-guided Spatiotemporal Attention Mechanism (SSAM) and Spatiotemporal Feature Sampling Strategy (STFS). In SSAM, we first use SNNs to perceive and accumulate temporal semantics. Then, with the help of historical temporal semantics, the semantics of the current moment are interacted and fused across time and space. Note that, in the time dimension, the event information of future moments is unknown. Therefore, in the process of enhancing the semantic meaning of the current moment, we do not consider the future spatial and temporal semantics. This design facilitates real-time computation in practical scenarios. To better leverage the advantages of SSAM, we introduce it at different levels of SEW-ResNet. With the help of SSAM and SEW-ResNet, isolated and discrete spatiotemporal semantics would be better correlated. In STFS, we randomly sample a number of large-sized patches in the spatial dimension to cover the original features and drive the model to perceive and capture effective semantics from each patch. Accordingly, we randomly collect event sub-sequences from the time dimension. The combination of these two strategies further enhances the model’s ability to capture robust semantics. STFS has no additional parameters and is only used during the training stage. Therefore,  $S^3$ CE-Net is a low-parameter and high-efficiency long-sequence event person Re-ID model. The main contributions of this paper are as follows:

- We proposed the SSAM to enhance the interaction and dependence of spatiotemporal semantics.
- We introduce the STFS to drive the Re-ID model to capture broader and more robust spatiotemporal semantics.
- Combined SSAM and STFS, we propose a simple and efficient long-sequence event ReID network,  $S^3$ CE-Net. Our  $S^3$ CE-Net achieves outstanding performance on

many mainstream long-sequence even ReID datasets.

## 2. Related Work

### 2.1. Video-Based Person Re-Identification

Video-based Person Re-identification (Re-ID)[26, 50, 61, 64] extends traditional Image-based Re-ID methods[5, 9, 11, 28–30, 34, 37] by leveraging the temporal information in videos to improve person matching accuracy. Compared to single-frame images, videos contain rich and useful information, including temporal and spatial features, as well as variations in body posture from different viewpoints.

*Global appearance-based methods* often aggregate multi-frame features into a single global feature vector using pooling[17, 36, 73] or recurrent neural networks (RNNs)[42, 45]. *To better preserve temporal information*, spatiotemporal attention mechanisms and graph convolutional networks (GCNs) have been introduced to enhance matching accuracy by focusing on key regions or establishing relationships between frames. Spatiotemporal attention mechanisms, such as the STA [15], focus on the most discriminative parts of the video, mitigating the effects of lighting changes and occlusion on recognition. Graph convolutional networks (e.g., SGGNN[6]) leverage graph structures to learn the similarity relationships between frames, enhancing the model’s robustness. Some studies also propose *local part alignment methods*, which extract features from local regions in the video to avoid misalignment between frames. For instance, spatiotemporal completion networks (STCnet)[25] tackle partial occlusion by recovering the appearance information of occluded parts. To extract fine-grained cues, [71] proposed Multi-Granularity Reference Assisted Feature Aggregation (MG-RAFA) to jointly process spatiotemporal features. Meanwhile, STT [70] adopted the *Transformer pattern* to enhance the representation of long-range temporal dependencies by processing relationships between frames.

### 2.2. Event-based Vision Tasks

As new types of sensors, in high-speed motion, event cameras can capture brightness changes with microsecond-level response times, effectively reducing motion blur[10, 52, 53, 63]. Their asynchronous data acquisition allows for lower latency and faster response in tasks such as Visual Odometry (VO)[31, 49, 75, 76] and SLAM[4, 62]. Besides, event cameras maintain excellent visual perception under high or low-light conditions. This enables event cameras to perform excellently in tasks such as optical flow estimation[12, 19, 32], object detection[48], and tracking[18, 33], helping achieve stable and reliable visual tasks under complex lighting conditions. For Re-ID, event cameras can reduce the leakage of person appearance information, and the imaging principle of event cameras can reduce the interference of

background information.

## 3. Methods

### 3.1. Overview

Our proposed Spike-guided Spatiotemporal Semantic Coupling and Expansion Network ( $S^3$ CE-Net) is illustrated in Fig. 3. We adopt the SEW-ResNet[14] as the backbone of our  $S^3$ CE-Net. The event tensor sequence is the input information for  $S^3$ CE-Net. The proposed  $S^3$ CE-Net contains the Spike-guided Spatiotemporal Attention Mechanism (SSAM) and Spatiotemporal Feature Sampling Strategy (STFS). The SSAM is designed to conduct semantic interaction and association in the spatial and temporal dimensions. To better leverage the advantages of SSAM, we integrate SSAM at different levels of SEW-ResNet. In the STFS, we sample patches in the spatial dimension and subsequences in the temporal dimension, driving the model to perceive the features of each region equally to capture robust semantics. The STFS is parameter-free and is applied only during the training stage to improve model robustness; SSAM is also built on SNNs. The computation of parameters only occurs in SSAM and the backbone SEW-ResNet. So,  $S^3$ CE-Net can be considered a lightweight network.

### 3.2. Event Representation

Event stream captured by the event camera is represented by a set  $E = \{e_i \mid i = 0, 1, 2, \dots, N\}$ , with a single event denoted as  $e_i = (x_i, y_i, t_i, p_i)$ , where  $x_i, y_i$  represent the spatial coordinates,  $t_i$  is the timestamp, and  $p_i$  indicates the direction of the brightness change (increase or decrease). To this, we divide the asynchronous event stream into a sequence of  $T$  tensors with fixed time intervals, where each tensor consists of two channels: one for positive polarity events and one for negative polarity events. So, the processed event tensors is  $X_e \in R^{T \times 2 \times W \times H}$ .

### 3.3. Backbone: SEW-ResNet

Spiking Neural Networks (SNNs) excel in processing event-driven data, such as the sparse and asynchronous signals generated by event cameras. Furthermore, SEW-ResNet[14] leveraged the Spike-Element-Wise Residual block (SEW-Resblock) to efficiently implement residual learning and stabilize gradient propagation. For this reason, we adopt SEW-ResNet as our  $S^3$ CE-Net’s backbone. Structure of SEW-Resblock is shown in Fig. 3-b. For more details about SEW-ResNet, refer to [14].

### 3.4. SSAM

As previously mentioned in Intro. 1, compared with CNNs and Transformers, SNNs are good at processing time-series event streams. However, event semantics are extremely discrete and isolated. SNNs are difficult to effectively model

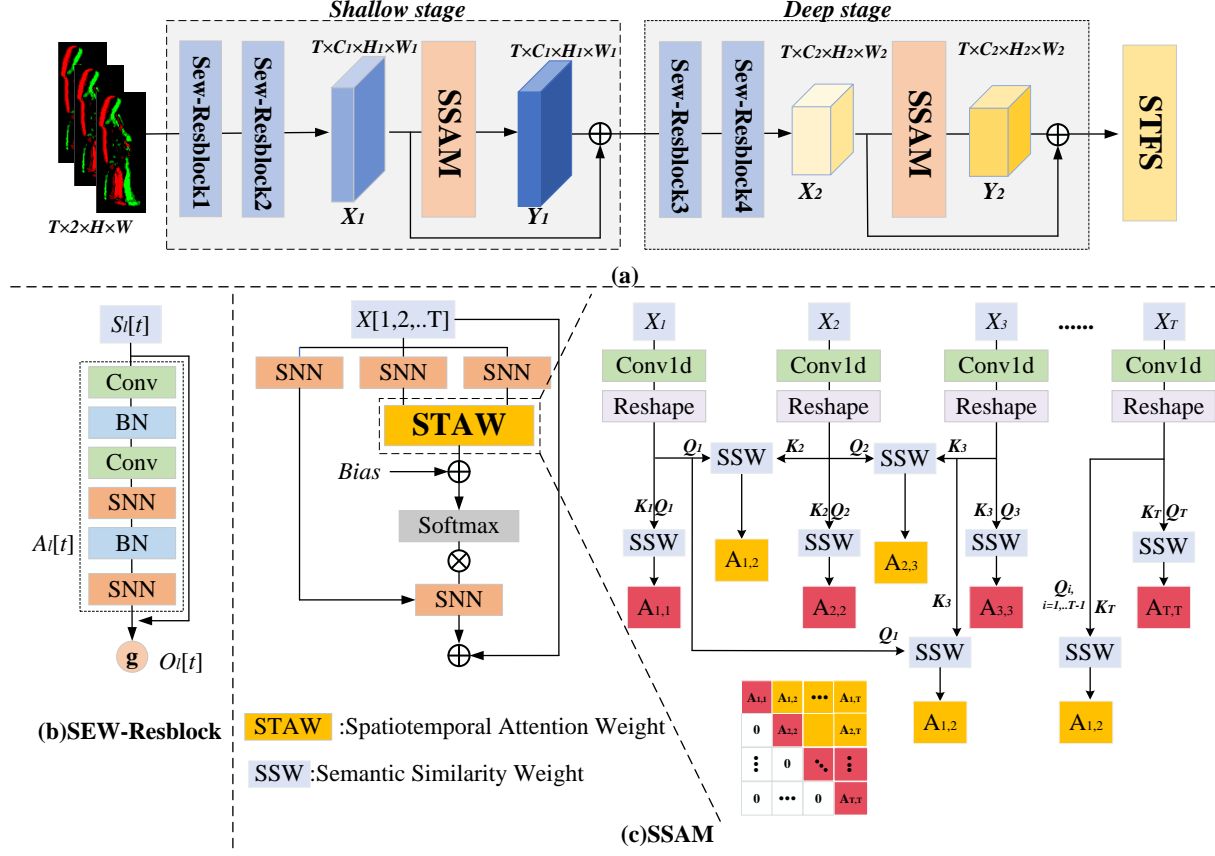


Figure 3. Overview of our S<sup>3</sup>CE-Net (a) which takes  $T$  event tensors as input, using SEW-ResNet18 as the backbone. It extracts features through four Spike-Element-Wise Residual blocks (SEW-Resblock) (b) and establishes spatiotemporal dependencies via the Spike-guided Spatiotemporal Attention Mechanism (SSAM) (c). Finally, the Spatiotemporal Feature Sampling Strategy (STFS) module drives model perceives broader and more robust effective semantics.

the association and dependence between discrete semantics. The compact contextual semantics is more conducive to driving the model to efficiently perceive and capture discriminative person semantics. Thus, based on SNNs, we further conduct spatiotemporal semantic association modeling to enhance the compactness between semantics. However, in the time dimension, the event information of future moments is unknown. Therefore, we only use historical temporal semantics to interact and integrate the semantic of events at the current moment. It differs from the Transformer, which performs semantic interaction across all time steps. This is more aligned with practical real-time application scenarios. To achieve the goal, we propose a Spike-guided Spatiotemporal Attention Mechanism (SSAM).

As shown in Fig. 3, to better leverage the advantages of SSAM, we introduce SSAM at two stages of SEW-ResNet. For the input feature  $X_s = (x_{s,1}, x_{s,2}, \dots, x_{s,T}) \in R^{T \times C_s \times H_s \times W_s}$ ,  $s \in \{1, 2\}$ , where  $x_{s,t}$  represents the event semantics corresponding to the  $t$ -th time step,  $s$  represents the  $s$ -th feature extraction stage of SEW-ResNet.

We first flatten feature  $X_s$  by  $X_s = Flatten(X_s) \in R^{T \times C_s \times (H_s \times W_s)}$ .

Then, we calculate the Spatiotemporal Attention Weight (STAW) (as shown in Fig. 3-c) by

$$Q_{s,global} = SNN_Q(Conv_{1d}(X_s)) \quad (1)$$

$$K_{s,global} = SNN_K(Conv_{1d}(X_s)) \quad (2)$$

$$V_{s,global} = SNN_V(Conv_{1d}(X_s)) \quad (3)$$

Where  $SNN_Q$ ,  $SNN_K$ , and  $SNN_V$  are separate SNN Layers with independent parameters,  $Conv_{1d}$  is the  $1 \times 1$  convolution operation,  $Q_{s,global}$ ,  $K_{s,global}$ , and  $V_{s,global} \in R^{T \times C_s \times N_s}$ ,  $N_s = H_s \times W_s$  are the global query, key, and value obtained through the  $s$ -th stage, representing the features across the entire temporal sequence. From  $Q_{s,global}$ ,  $K_{s,global}$ , and  $V_{s,global}$ , we extract the query, key, and value for each tensor  $t$ -th time step as:  $Q_{s,t} = Q_{s,global}[t, :, :]$ ,  $K_{s,t} = K_{s,global}[t, :, :]$ , and  $V_{s,t} = V_{s,global}[t, :, :]$ , where  $Q_{s,t}$ ,  $K_{s,t}$ ,  $V_{s,t} \in R^{C_s \times N_s}$  represent the query, key, and value for event tensor  $t$ ,  $t \in \{1, 2, \dots, T\}$  is the time step



index,  $N_s = H_s \times W_s$  represents the number of tokens per event tensor.

To capture the spatial relationships among  $N_s$  tokens within an event tensor  $x_{s,t}$ , we introduce a learnable intra-frame relative position bias  $B \in R^{N_s \times N_s}$ , which captures the spatial dependencies within a single event tensor. A detailed formulation of  $B$  and its implementation is provided in Section A of Supplementary Materials.

When computing the attention matrix, each event tensor at a given time step interacts only with tensors from the current and previous time steps. This is because the value weights of future tensor information with respect to current information are unknown, ensuring temporal consistency in the model and aligning with the real-world understanding of dynamic scenes. This is different from the previous Transformer idea and will effectively reduce the amount of computation. For the convenience of expression, we omit the variable  $s$  in the tensor calculation stage without causing ambiguity. So, the similarity weight of the event tensor at the  $t'$ -th time step and the event tensor at the  $t$ -th time step (current time step) is calculated as:

$$A_{t',t} = \begin{cases} \frac{Q_{t'} \cdot K_t^T}{\sqrt{D}} & \text{if } t' < t \\ \frac{Q_{t'} \cdot K_t^T}{\sqrt{D}} + B & \text{if } t' = t \\ 0 & \text{if } t' > t \end{cases} \quad (4)$$

Here, for the current time step  $t$ , when  $t' \leq t$ , we retain the calculated weight, otherwise, the weight is reset to 0 to discard the influence of future event tensors on the current moment. Since this, the STAW shown in Fig. 3-(c) is the final similarity weight matrix we calculate. We can clearly see that the weight matrix is an upper triangular matrix.

Finally, based on such a weight matrix, we perform interaction and fusion between spatiotemporal semantics by

$$O_t = SNN\left(\sum_{t'=1}^t \text{Softmax}(A_{t',t}, \text{dim} = -1) \cdot V_t\right) \quad (5)$$

where  $O_t \in R^{C_s \times N_s}$  represents the output that fuses the past spatiotemporal semantic information related to the  $t$ -th event tensor. The final output is obtained by concatenating the outputs of all event tensors:

$$Y_s = [O_1; O_2; \dots; O_T] \in R^{T \times C_s \times N_s} \quad (6)$$

### 3.5. STFS

As mentioned in Intro. 1, deep models can easily fall into local effective semantics, ignoring perception of broader effective semantics. To this, we try to use sub-regions and sub-sequences from the spatial and temporal dimensions to drive deep models to perceive broader effective semantics. So, we propose the Spatiotemporal Feature Sampling Strategy (STFS). Schematic diagram of STFS is shown in Fig. 4.

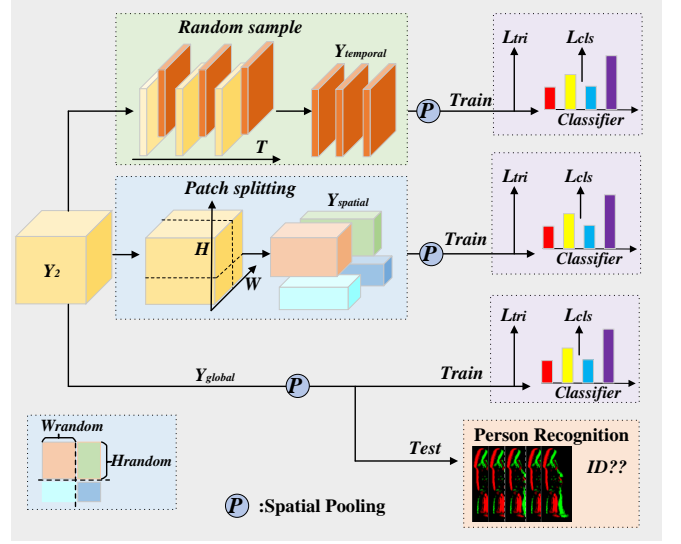


Figure 4. Architecture of the proposed STFS. For different branch, we use triplet loss and label smoothing cross-entropy loss for constraints, represented by  $L_{tri}$  and  $L_{cls}$ .

To reduce the computational load and effectively feed back the training of the entire network, our STFS is applied on the deep feature map  $Y_2$ . As shown in Fig. 4, from top to bottom, they are subsequence sampling in the time dimension, subregion sampling in the spatial dimension, and the extraction branch of global semantic descriptors.

**Subsequence Sampling in the Time Dimension:** As shown in top branch of Fig. 4, we randomly select  $k = \frac{T}{2}$  time steps  $T_{random} \subset \{1, 2, \dots, T\}$ , which can be represented as:

$$T_{random} = \{t_1, t_2, \dots, t_k\} \quad (7)$$

Perform average pooling on each selected time step to obtain the feature representation corresponding to each random time step.

$$Y_{temporal} = \{V_{t_i} \mid t_i \in T_{random}\} \quad (8)$$

$$V_{t_i} = \text{Avg2d}(Y_2[t_i, :, :, :])$$

where  $Y_{temporal}$  represents the randomly selected subsequence samples' semantics in the time dimension,  $\text{Avg2d}$  refers to the 2D average pooling operation.

**Subregion Sampling in the Spatial Dimension:** The feature map is divided into four random patches, and average pooling is performed separately on each patch. The average pooling operation in each patch results in a feature vector that represents the features of the local region.

$$Y_{spatial} = \{V_{ul}, V_{ur}, V_{ll}, V_{lr}\}, \quad (9)$$

$$V_{ul} = \text{Avg2d}(Y_2[:, :, : W_{random}, : H_{random}]).$$

where  $ul, ur, ll, lr$  denote the upper left, upper right, lower left, and lower right feature regions respectively;

Table 1. Performance (%) comparison with various SOTA methods on MARS, PRID-2011, and iLIDS-VID datasets.

Methods		MARS		PRID-2011		iLIDS-VID	
Network	Input	mAP	Rank-1	mAP	Rank-1	mAP	Rank-1
GRL[40]	E	24.7	16.7	22.3	11.8	25.2	13.2
OSNet[74]	E	20.9	19.3	22.2	10.1	23.7	12.6
SRS-Net[57]	E	17.9	10.6	19.2	11.3	20.7	9.3
STMN[13]	E	22.4	10.9	20.2	11.2	21.1	10.4
CTL[39]	E	19.6	12.7	20.4	12.4	24.1	12.5
PSTA[60]	E	22.7	12.0	21.4	12.5	22.4	10.0
FastReID[23]	E	39.3	26.2	65.8	54.1	41.8	29.6
SDCL [3]	E	38.3	26.8	61.1	50.7	43.1	30.7
VSLA-CLIP [69]	E	33.4	20.9	57.5	45.3	36.9	26.6
TF-CLIP[68]	E	41.9	29.7	64.7	52.4	44.2	32.6
CMTC[35]	E	43.8	31.6	71.9	60.4	47.5	35.3
Ours	E	<b>67.4</b>	<b>55.2</b>	<b>90.3</b>	<b>80.9</b>	<b>71.0</b>	<b>58.8</b>

$W_{random}$  and  $H_{random}$  are obtained by random sampling on  $[0, W_2]$ ,  $[0, H_2]$  respectively. Similarly, the other regions—upper right ( $V_{ur}$ ), lower left ( $V_{ll}$ ), and lower right ( $V_{lr}$ )—are obtained by performing average pooling on the corresponding patches of the feature map.

**Global Semantic Extraction:** At the 2-th stage, we restore the feature  $Y_2$  to its spatiotemporal dimensions, and obtain the global semantic vector by

$$Y_2 = Reshape(Y_2) \in R^{T \times C_2 \times H_2 \times W_2}, \quad (10)$$

$$Y_{global} = Avg2d(Y_2[:, :, :, :]).$$

During the training phase, we use triplet loss  $L_{tri}$  and cross-entropy loss with label smoothing  $L_{cls}$  to constrain  $Y_{temporal}$ ,  $Y_{spatial}$ , and  $Y_{global}$ . The loss function of our  $S^3$ CE-Net is summarized as  $L_{total} = \lambda_1 L_{tri} + \lambda_2 L_{cls}$ . The  $\lambda_1 = 1.0$  and  $\lambda_2 = 0.1$  represent the weights of different losses. During the testing stage, we only use the global semantic vector  $Y_{global}$  to conduct the person matching.

## 4. Experiments

### 4.1. Datasets

Currently, there is no event-based long-sequence ReID dataset. We first follow Cao’s[3] to adopt the Video-to-Event [27] method for generating event streams from three classic video-based person Re-ID datasets, **PRID-2011**[24], **iLIDS-VID**[58], and **MARS**[73]. In addition, we conduct experiments on the first *real* event-camera dataset for Re-ID, namely **Event-ReID**[1]. Event-ReID was captured by four indoor  $640 \times 480$  Prophesee cameras and contains 33 identities walking across the four views. After hand-crafted and YOLO-assisted annotation, we obtain 16k bounding boxes that form long event streams suitable for sequence-level evaluation. Comprehensive statistics, annotation protocol and preprocessing details are pro-

Table 2. Performance (%) on the *Event-ReID* dataset.

Method	mAP	Rank-1
ResNet-18	71.2	60.5
<b>Ours</b>	<b>93.7</b>	<b>86.3</b>

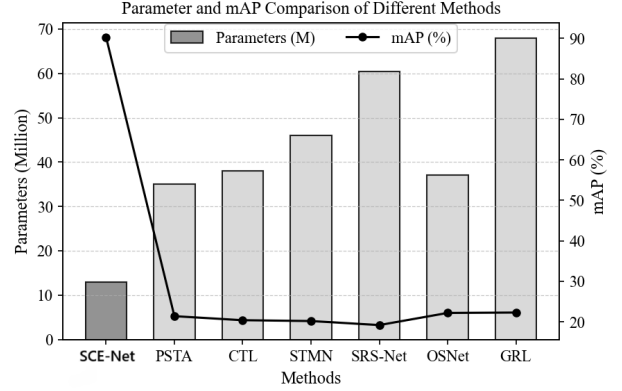


Figure 5. Parameters and mAP (in %) comparison.

vided in the Supplementary Materials.

### 4.2. Implementation Details

Our network is implemented based on the PyTorch deep learning framework on a single NVIDIA RTX 2080Ti GPU. The training process lasts for 100 epochs, with an initial learning rate of 0.00035, which is decayed to one-third of its original value every 30 epochs. The Adam optimizer is used for parameter updates. During the testing phase, cosine similarity is employed to measure the distance between gallery and query instances.

### 4.3. Comparison with SOTA methods

Table 1 shows the performance of our proposed method for event-driven video person re-identification on MARS, PRID-2011, and iLIDS-VID datasets. Due to the scarcity of existing event-driven video person re-identification methods, we will retrain and test the previous RGB-based ReID model with event data. As shown in Table 1, our network achieves excellent performance across multiple public datasets, further demonstrating its advanced nature and effectiveness on event data. The experimental results indicate that current methods developed for RGB data do not perform well with asynchronous event data. Besides, Fig. 5 clearly demonstrates that our  $S^3$ CE-Net achieves higher accuracy with fewer parameters compared to other methods.

To further demonstrate the robustness of the model under blurred conditions, we followed Cao’s[3] method to introduce blur into the PRID-2011 and iLIDS-VID datasets to simulate scenarios with fast motion. As shown in Table 3, for a fair comparison, the experiments for other SOTA

Table 3. The mAP(%) values of different methods on PRID-2011, and iLIDS-VID datasets in blurry conditions.

Methods		PRID-2011	iLIDS-VID
Network	Input	Blurry	Blurry
GRL[40]	V	81.8	60.7
SRS-Net[57]	V	78.8	61.6
STMN[13]	V	81.5	57.7
CTL[39]	V	81.6	56.0
PSTA[60]	V	79.7	58.9
GRL[40]	V+E	88.4	66.2
SRS-Net[57]	V+E	82.1	67.8
STMN[13]	V+E	85.5	62.3
CTL[39]	V+E	88.6	64.2
PSTA[60]	V+E	85.0	65.5
SDCL[3]	V+E	89.5	<b>71.4</b>
Ours	E	<b>90.1</b>	70.4

methods were divided into two groups: the first group used the original RGB Video data as input (i.e. V), and the second group used both RGB and Event data as input (i.e. V+E). The experimental results in Table 3 clearly demonstrate the advantages of event data under degraded conditions. On the PRID dataset, our method achieved the best performance, highlighting the rationality of our model framework designed specifically for event data. Limited by the fact that event data is more sparse and has lower information density compared to RGB data, coupled with the frequent person occlusions in the iLIDS-VID dataset, the extraction of target features becomes constrained, increasing the difficulty of feature extraction and recognition. Consequently, compared to the SDCL[3], we achieved comparable performance levels using only event data. This means that our model can mine effective person semantics from event streams for person matching.

#### 4.4. Experimental on the Real Event-ReID Dataset

On the real Event-ReID dataset (Table 2), our method surpasses the ResNet-18 baseline by 22.5 pp in mAP and 25.8 pp in Rank-1, confirming the efficacy of SSAM and STFS on sparse event streams. SSAM extracts coherent spatiotemporal semantics and suppresses noise, STFS randomly samples diverse sub-blocks to mitigate over-fitting, and the event-driven SNN naturally matches asynchronous data. As Event-ReID contains only 33 identities, future work will validate generalisation on larger, cross-scene datasets.

#### 4.5. Ablation Study

##### 4.5.1. Effectiveness of SNN:

In our S<sup>3</sup>CE-Net, we employed a SNN to extract person feature from event streams. To validate the rationality and effectiveness of introducing SNNs, we performed ablation

Table 4. Impact of different Baselines on Re-ID performance.

Network	PRID-2011	iLIDS-VID
Sew-Resnet	61.9	50.2
Resnet-18	35.5	31.2
Resnet-50	32.0	30.3

Table 5. Results produced by combining different mechanisms in the S<sup>3</sup>CE-Net.

SSAM	STFS	PRID-2011		iLIDS-VID	
		mAP	rank-1	map	rank-1
w/o	w/o	61.9	52.0	50.2	43.3
w	w/o	80.2	73.3	65.6	57.0
w/o	w	67.0	56.1	51.2	45.5
w	w	<b>90.3</b>	<b>80.9</b>	<b>71.0</b>	<b>58.8</b>

Table 6. The ablation study results demonstrating the impact of incorporating SSAM at various stages.

SSAM	Shallow-stage	Deep-stage	PRID-2011		iLIDS-VID	
			mAP	rank-1	mAP	rank-1
	-	-	67.0	56.1	51.2	45.5
	✓	-	86.3	77.2	63.3	52.3
	-	✓	85.7	76.0	64.8	53.2
	✓	✓	<b>90.3</b>	<b>80.9</b>	<b>71.0</b>	<b>58.8</b>

experiments by replacing the SNN model with a classic ResNet. The experimental results in Table 4 indicate that as the network depth increases, the performance of the model is gradually declining. This suggests that SNNs possess a superior capability for capturing and extracting event semantics in comparison to CNNs.

##### 4.5.2. Effectiveness of SSAM and STFS:

The SSAM is designed to enhance the interaction and dependence of spatiotemporal semantics. The STFS is designed to drive model perceives broader and more robust effective semantics. The results are reported in Table 5. As shown in Table 5, we can clearly see that SSAM and STFS have significant contributions to the performance of S<sup>3</sup>CE-Net. The numerical experimental results significantly verify the effectiveness of the two designs.

##### 4.5.3. Discussion on SSAM

We firstly validate its effectiveness at different stages of feature extraction. As shown in Table 6 and Fig. 3, when the SSAM module is applied only to the shallow or deep stage, the model performance improves significantly compared to when the module is not applied. Specifically, for complex Re-ID datasets like iLIDS-VID, the performance improvement is more pronounced across both stages. This suggests that in practical applications, the stages for adding the SSAM module can be flexibly chosen based on the dataset

Table 7. Results of Ablation Study on Attention Matrix in SSAM Module, STAW represents the Spatiotemporal Attention Weight shown in Fig 3-c, FAW represents the Full Attention Weight, where each time tensor computes attention with other tensors, and ZAW represents the Zero Attention Weight, where all attention weights are zero.

Strategy	PRID		iLIDS-VID	
	MAP	Rank-1	MAP	Rank-1
STAW	<b>90.3</b>	<b>80.9</b>	<b>71</b>	<b>58.8</b>
FAW	87.6	77.8	68.1	55.3
ZAW	67.0	56.1	51.2	45.5

Table 8. Ablation study results demonstrate the impact of the temporal and spatial branches in STFS.

STFS	Spatial	Temporal	PRID-2011		iLIDS-VID	
			mAP	rank-1	mAP	rank-1
	✓	-	88.1	78.2	67.8	56.2
	-	✓	89.3	79.8	68.2	57.7
	✓	✓	<b>90.3</b>	<b>80.9</b>	<b>71.0</b>	<b>58.8</b>

characteristics and computational cost. To validate the effectiveness of the *Spatiotemporal Attention Weight (STAW)* in SSAM module, we compared it with commonly used Full Attention Weights (where each time tensor computes attention with all other tensors, i.e. FAW in Table 7) and Zero Attention Weights (ZAW in Table 7). The experimental results 7 demonstrate that attention computation significantly improves recognition accuracy, with the design of our STAW achieving the best performance.

#### 4.5.4. Discussion on STFS

We validated the contributions of its temporal and spatial branches to the model. Table 8 demonstrates that random sampling of temporal and spatial features in the final stage enhances the model’s robustness without increasing its parameter size. This performance enhancement is attributed to the STFS-driven model, which expands the perception and capture range of effective semantics, thereby enhancing the robustness of semantics.

#### 4.5.5. Visualization of Retrieval Results:

In Fig 6, we visualize the retrieval results of our S<sup>3</sup>CE-Net compared to Baseline. In some cross-scene person retrieval tasks, our model successfully retrieves video sequences of the same person in different scenes, whereas the baseline retrieves incorrect cross-scene person sequences. This comparison highlights the superior performance of S<sup>3</sup>CE-Net.

#### 4.6. Domain Generalization Evaluation

In this part, we compare the domain generalization performance of our S<sup>3</sup>CE-Net in the RGB modality and the event

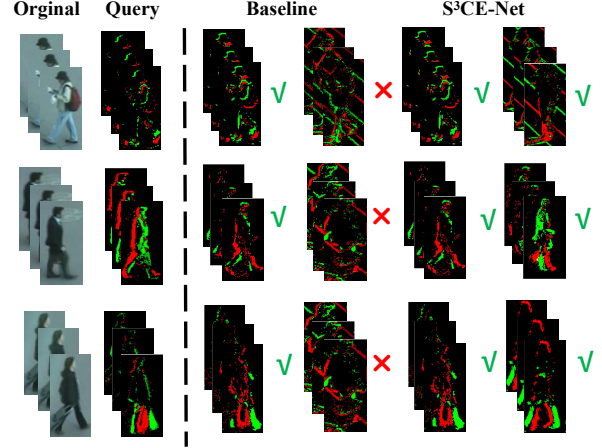


Figure 6. Visualization of the retrieval results using Baseline and S<sup>3</sup>CE-Net. The first and second columns represent the RGB and temporal images of the queried person under camera 1, the third and fourth columns respectively display the retrieval results from the baseline model under camera 1 and camera 2, and the fifth and sixth columns respectively display the retrieval results from S<sup>3</sup>CE-Net under camera 1 and camera 2. Correct matches and incorrect matches are indicated by check marks and crosses, respectively.

Table 9. Single-domain vs. Cross-domain evaluations (mAP and performance drop) on the blurred dataset, across Event and RGB modalities. “Ref. Value” (Reference Value) represents the model’s training and testing on the target dataset.

Modality	Training Dataset	Test Dataset & Performance		
		Blurry	mAP	Drop
Event	PRID-2011	Ref. Value	70.4	-
		iLIDS-VID	64.4	-6.0
Event	iLIDS-VID	Blurry	mAP	Drop
		Ref. Value	90.1	-
		PRID-2011	83.2	-6.9
RGB	PRID-2011	Blurry	mAP	Drop
		Ref. Value	62.2	-
		iLIDS-VID	51.5	-10.7
RGB	iLIDS-VID	Blurry	mAP	Drop
		Ref. Value	79.7	-
		PRID-2011	67.4	-12.3

modality. In addition, we further blur the unknown target domain data to simulate blur caused by high-speed motion or camera shake. This further increases the difficulty of model domain generalization.

- Train the model on the standard PRID dataset and tested it on the unseen blurred iLIDS-VID dataset.
- Train the model on the standard iLIDS-VID dataset and tested it on the unseen blurred PRID dataset.

As shown in Table 9, compared to single-domain testing, the performance of the model in the domain generalization task decreases in both RGB and Event modalities. How-



ever, compared to the RGB modality, the model is trained on event data, resulting in higher performance and less performance degradation during domain generalization. This also verifies that compared to the RGB modality, the event modality is beneficial for improving the generalization performance of the Re-ID domain. This is because RGB data often contains a large amount of background information and scene style information, which are important obstacles to model domain generalization. The event camera can better shield these two parts of information.

## 5. Conclusion

In this paper, we proposed a Spike-guided Spatiotemporal Semantic Coupling and Expansion Network ( $S^3$ CE-Net) for the long-sequence event Re-ID task. Our  $S^3$ CE-Net is build on the spiking neural networks (SNNs). The  $S^3$ CE-Net contains the Spike-guided Spatial-temporal Attention Mechanism (SSAM) and Spatiotemporal Feature Sampling Strategy (STFS). The SSAM conducted the semantic interaction and association in the spatial and temporal dimensions. The STFS drove the Re-ID model's ability to capture robust semantics from spatiotemporal dimensions. Extensive experiments have verified that our  $S^3$ CE-Net achieves outstanding performance on many mainstream long-sequence event person Re-ID datasets.

## References

- [1] Shafiq Ahmad, Pietro Morerio, and Alessio Del Bue. Person re-identification without identification via event anonymization. In *2023 IEEE/CVF International Conference on Computer Vision (ICCV)*, pages 11098–11107, 2023. 6
- [2] N. Burkitt. A review of the integrate-and-fire neuron model: I. homogeneous synaptic input. *Biol. Cybern.*, 95(1):1–19, 2006. 13
- [3] Chengzhi Cao, Xueyang Fu, Hongjian Liu, Yukun Huang, Kunyu Wang, Jiebo Luo, and Zheng-Jun Zha. Event-guided person re-identification via sparse-dense complementary learning. In *2023 IEEE/CVF Conference on Computer Vision and Pattern Recognition (CVPR)*, pages 17990–17999, 2023. 6, 7
- [4] William Chamorro, Joan Solà, and J. Andrade-Cetto. Event-based line slam in real-time. *IEEE Robotics and Automation Letters*, 7:8146–8153, 2022. 3
- [5] Binghui Chen, Weihong Deng, and Jiani Hu. Mixed high-order attention network for person re-identification. In *2019 IEEE/CVF International Conference on Computer Vision (ICCV)*, pages 371–381, 2019. 3
- [6] Dapeng Chen, Dan Xu, Hongsheng Li, Nicu Sebe, and Xiaogang Wang. Group consistent similarity learning via deep crf for person re-identification. In *2018 IEEE/CVF Conference on Computer Vision and Pattern Recognition*, pages 8649–8658, 2018. 3
- [7] Guangyi Chen, Jiwen Lu, Ming Yang, and Jie Zhou. Spatial-temporal attention-aware learning for video-based person re-identification. *IEEE Transactions on Image Processing*, 28(9):4192–4205, 2019. 1, 2
- [8] Guangyi Chen, Jiwen Lu, Ming Yang, and Jie Zhou. Learning recurrent 3d attention for video-based person re-identification. *IEEE Transactions on Image Processing*, 29:6963–6976, 2020. 1
- [9] Xiaodong Chen, Xinchun Liu, Wu Liu, Xiao-Ping Zhang, Yongdong Zhang, and Tao Mei. Explainable person re-identification with attribute-guided metric distillation. In *2021 IEEE/CVF International Conference on Computer Vision (ICCV)*, pages 11793–11802, 2021. 3
- [10] Hoonhee Cho, Yuhwan Jeong, Taewoo Kim, and Kuk-Jin Yoon. Non-coaxial event-guided motion deblurring with spatial alignment. In *2023 IEEE/CVF International Conference on Computer Vision (ICCV)*, pages 12458–12469, 2023. 3
- [11] Seokeon Choi, Taekyung Kim, Minki Jeong, Hyungseob Park, and Changick Kim. Meta batch-instance normalization for generalizable person re-identification. In *2021 IEEE/CVF Conference on Computer Vision and Pattern Recognition (CVPR)*, pages 3424–3434, 2021. 3
- [12] Ziluo Ding, Rui Zhao, Jiyuan Zhang, Tianxiao Gao, Ruiqin Xiong, Zhaoqi Yu, and Tiejun Huang. Spatio-temporal recurrent networks for event-based optical flow estimation. In *AAAI Conference on Artificial Intelligence*, 2021. 3
- [13] Chanhoe Eom, Geon Lee, Junghyup Lee, and Bumsub Ham. Video-based person re-identification with spatial and temporal memory networks. *2021 IEEE/CVF International Conference on Computer Vision (ICCV)*, pages 12016–12025, 2021. 6, 7
- [14] Wei Fang, Zhaoqi Yu, Yanqing Chen, Tiejun Huang, Timothée Masquelier, and Yonghong Tian. Deep residual learning in spiking neural networks. In *Neural Information Processing Systems*, 2021. 2, 3
- [15] Yang Fu, Xiaoyang Wang, Yunchao Wei, and Thomas Huang. Sta: Spatial-temporal attention for large-scale video-based person re-identification. *Proceedings of the AAAI Conference on Artificial Intelligence*, 33(01):8287–8294, 2019. 3
- [16] Guillermo Gallego, Tobi Delbrück, Garrick Orchard, Chiara Bartolozzi, Brian Taba, Andrea Censi, Stefan Leutenegger, Andrew J. Davison, Jörg Conradt, Kostas Daniilidis, and Davide Scaramuzza. Event-based vision: A survey. *IEEE Transactions on Pattern Analysis and Machine Intelligence*, 44(1):154–180, 2022. 1
- [17] Jiyang Gao and Ram Nevatia. Revisiting temporal modeling for video-based person reid. 2018. 3
- [18] Daniel Gehrig, Henri Rebecq, Guillermo Gallego, and Davide Scaramuzza. Ekl: Asynchronous photometric feature tracking using events and frames. *International Journal of Computer Vision*, 128:601 – 618, 2018. 3
- [19] Mathias Gehrig, Mario Millhäusler, Daniel Gehrig, and Davide Scaramuzza. E-raft: Dense optical flow from event cameras. *2021 International Conference on 3D Vision (3DV)*, pages 197–206, 2021. 3
- [20] Golnaz Ghiasi, Tsung-Yi Lin, and Quoc V Le. Dropblock: A regularization method for convolutional networks. In *arXiv:1810.12890*, 2018. 2
- [21] Xinqian Gu, Hong Chang, Bingpeng Ma, Hongkai Zhang, and Xilin Chen. Appearance-preserving 3d convolution for

- video-based person re-identification. In *Computer Vision – ECCV 2020*, pages 228–243, Cham, 2020. Springer International Publishing. 1, 2
- [22] Ali Hassani, Steven Walton, Jiachen Li, Shen Li, and Humphrey Shi. Neighborhood attention transformer. In *IEEE/CVF Conference on Computer Vision and Pattern Recognition, CVPR 2023, Vancouver, BC, Canada, June 17–24, 2023*, pages 6185–6194. IEEE, 2023. 2
- [23] Lingxiao He, Xingyu Liao, Wu Liu, Xinchun Liu, Peng Cheng, and Tao Mei. Fastreid: A pytorch toolbox for general instance re-identification. *Proceedings of the 31st ACM International Conference on Multimedia*, 2020. 6
- [24] Martin Hirzer, Csaba Beleznai, Peter M. Roth, and Horst Bischof. Person re-identification by descriptive and discriminative classification. In *Proceedings of the 17th Scandinavian Conference on Image Analysis*, page 91–102, Berlin, Heidelberg, 2011. Springer-Verlag. 6
- [25] Ruibing Hou, Bingpeng Ma, Hong Chang, Xinqian Gu, Shiguang Shan, and Xilin Chen. VRSTC: Occlusion-Free Video Person Re-Identification. In *2019 IEEE/CVF Conference on Computer Vision and Pattern Recognition (CVPR)*, pages 7176–7185, Los Alamitos, CA, USA, 2019. IEEE Computer Society. 3
- [26] Ruibing Hou, Hong Chang, Bingpeng Ma, Shiguang Shan, and Xilin Chen. Temporal complementary learning for video person re-identification. In *Computer Vision – ECCV 2020*, pages 388–405, Cham, 2020. Springer International Publishing. 3
- [27] Yuhuang Hu, Shih-Chii Liu, and Tobi Delbruck. v2e: From video frames to realistic dvs events. In *2021 IEEE/CVF Conference on Computer Vision and Pattern Recognition Workshops (CVPRW)*, pages 1312–1321, 2021. 6
- [28] Meiyang Huang, Chunping Hou, Qingyuan Yang, and Zhipeng Wang. Reasoning and tuning: Graph attention network for occluded person re-identification. *IEEE Transactions on Image Processing*, 32:1568–1582, 2023. 3
- [29] Yan Huang, Qiang Wu, JingSong Xu, Yi Zhong, and ZhaoXiang Zhang. Clothing status awareness for long-term person re-identification. In *2021 IEEE/CVF International Conference on Computer Vision (ICCV)*, pages 11875–11884, 2021.
- [30] Kunho Kim, Min-Jae Kim, Hyungtae Kim, Seokmok Park, and Joonki Paik. Person re-identification method using text description through clip. In *2023 International Conference on Electronics, Information, and Communication (ICEIC)*, pages 1–4, 2023. 3
- [31] Simone Klenk, Marvin Motzet, Lukas Koestler, and Daniel Cremers. Deep event visual odometry. *2024 International Conference on 3D Vision (3DV)*, pages 739–749, 2023. 3
- [32] Chankyu Lee, Adarsh Kosta, Alex Zihao Zhu, Kenneth Chaney, Kostas Daniilidis, and Kaushik Roy. Spike-flownet: Event-based optical flow estimation with energy-efficient hybrid neural networks. *ArXiv*, abs/2003.06696, 2020. 3
- [33] Gregor Lenz, Sio-Hoi Ieng, and Ryad Benosman. Event-based face detection and tracking using the dynamics of eye blinks. *Frontiers in neuroscience*, 14:587, 2020. 3
- [34] Hanjun Li, Gaojie Wu, and Wei-Shi Zheng. Combined depth space based architecture search for person re-identification. In *2021 IEEE/CVF Conference on Computer Vision and Pattern Recognition (CVPR)*, pages 6725–6734, 2021. 3
- [35] Renkai Li, Xin Yuan, Wei Liu, and Xin Xu. Event-based video person re-identification via cross-modality and temporal collaboration. *ArXiv*, abs/2501.07296, 2025. 6
- [36] Shuang Li, Slawomir Bak, Peter Carr, and Xiaogang Wang. Diversity regularized spatiotemporal attention for video-based person re-identification. In *2018 IEEE/CVF Conference on Computer Vision and Pattern Recognition*, pages 369–378, 2018. 3
- [37] Yangyang Li, Zichen Yang, Yanqiao Chen, Danqing Yang, Ruijiao Liu, and Licheng Jiao. Occluded person re-identification method based on multiscale features and human feature reconstruction. *IEEE Access*, 10:98584–98592, 2022. 3
- [38] Songnan Lin, Jiawei Zhang, Jinshan Pan, Zhe Jiang, Dongqing Zou, Yongtian Wang, Jing Chen, and Jimmy Ren. Learning event-driven video deblurring and interpolation. In *Computer Vision – ECCV 2020*, pages 695–710, Cham, 2020. Springer International Publishing. 1
- [39] Jiawei Liu, Zhengjun Zha, Wei Wu, Kecheng Zheng, and Qibin Sun. Spatial-temporal correlation and topology learning for person re-identification in videos. *2021 IEEE/CVF Conference on Computer Vision and Pattern Recognition (CVPR)*, pages 4368–4377, 2021. 6, 7
- [40] Xuehu Liu, Pingping Zhang, Chenyang Yu, Huchuan Lu, and Xiaoyun Yang. Watching you: Global-guided reciprocal learning for video-based person re-identification. *2021 IEEE/CVF Conference on Computer Vision and Pattern Recognition (CVPR)*, pages 13329–13338, 2021. 6, 7
- [41] Xuehu Liu, Chenyang Yu, Pingping Zhang, and Huchuan Lu. Deeply coupled convolution–transformer with spatial–temporal complementary learning for video-based person re-identification. *IEEE Transactions on Neural Networks and Learning Systems*, 35(10):13753–13763, 2024. 1
- [42] Yiheng Liu, Zhenxun Yuan, Wengang Zhou, and Houqiang Li. Spatial and temporal mutual promotion for video-based person re-identification. *Proceedings of the AAAI Conference on Artificial Intelligence*, 33(01):8786–8793, 2019. 3
- [43] Ze Liu, Yutong Lin, Yue Cao, Han Hu, Yixuan Wei, Zheng Zhang, Stephen Lin, and Baining Guo. Swin transformer: Hierarchical vision transformer using shifted windows. *2021 IEEE/CVF International Conference on Computer Vision (ICCV)*, pages 9992–10002, 2021. 13
- [44] Wolfgang Maass. Networks of spiking neurons: The third generation of neural network models. *Neural Networks*, 10(9):1659–1671, 1997. 2
- [45] Niall McLaughlin, Jesus Martinez del Rincon, and Paul Miller. Recurrent convolutional network for video-based person re-identification. In *2016 IEEE Conference on Computer Vision and Pattern Recognition (CVPR)*, pages 1325–1334, 2016. 3
- [46] Willi Menapace, Aliaksandr Siarohin, Ivan Skorokhodov, Ekaterina Deyneka, Tsai-Shien Chen, Anil Kag, Yuwei Fang, Aleksei Stoliar, Elisa Ricci, Jian Ren, and Sergey Tulyakov. Snap video: Scaled spatiotemporal transformers for text-to-video synthesis. In *IEEE/CVF Conference*

- on *Computer Vision and Pattern Recognition, CVPR 2024, Seattle, WA, USA, June 16-22, 2024*, pages 7038–7048. IEEE, 2024. 2
- [47] Paul A Merolla, John V Arthur, Rodrigo Alvarez-Icaza, Andrew S Cassidy, Jun Sawada, Filipp Akopyan, Bryan L Jackson, Nabil Imam, Chen Guo, Yutaka Nakamura, Bernard Brezzo, Ivan Vo, Steven K Esser, Rathinakumar Appuswamy, Brian Taba, Arnon Amir, Myron D Flickner, William P Risk, Rajit Manohar, and Dharmendra S Modha. Artificial brains: a million spiking-neuron integrated circuit with a scalable communication network and interface. *Science (New York, N.Y.)*, 345(6197):668–673, 2014. 2
- [48] Anton Mitrokhin, Cornelia Fermüller, Chethan Parameshwara, and Yiannis Aloimonos. Event-based moving object detection and tracking. In *2018 IEEE/RSJ International Conference on Intelligent Robots and Systems (IROS)*, pages 1–9, 2018. 3
- [49] Elias Mueggler, Guillermo Gallego, Henri Rebecq, and Davide Scaramuzza. Continuous-time visual-inertial odometry for event cameras. *IEEE Transactions on Robotics*, 34:1425–1440, 2017. 3
- [50] Minh Shim, Hsuan-I Ho, Jinhyung Kim, and Dongyoon Wee. Read: Reciprocal attention discriminator for image-to-video re-identification. In *Computer Vision – ECCV 2020*, pages 335–350, Cham, 2020. Springer International Publishing. 3
- [51] Nitish Srivastava, Geoffrey Hinton, Alex Krizhevsky, Ilya Sutskever, and Ruslan Salakhutdinov. Dropout: a simple way to prevent neural networks from overfitting. In *JMLR*, 2014. 2
- [52] Lei Sun, Christos Sakaridis, Jingyun Liang, Qi Jiang, Kailun Yang, Peng Sun, Yaozu Ye, Kaiwei Wang, and Luc Van Gool. Event-based fusion for motion deblurring with cross-modal attention. In *Computer Vision – ECCV 2022*, pages 412–428, Cham, 2022. Springer Nature Switzerland. 3
- [53] Lei Sun, Christos Sakaridis, Jingyun Liang, Peng Sun, Kai Zhang, Jie Zhang Cao, Qi Jiang, Kaiwei Wang, and Luc Van Gool. Event-based frame interpolation with ad-hoc deblurring. In *2023 IEEE/CVF Conference on Computer Vision and Pattern Recognition (CVPR)*, pages 18043–18052, 2023. 3
- [54] Yifan Sun, Liang Zheng, Yi Yang, Qi Tian, and Shengjin Wang. Beyond part models: Person retrieval with refined part pooling (and a strong convolutional baseline). In *Proceedings of the European Conference on Computer Vision (ECCV)*, 2018. 2
- [55] Jonathan Tompson, Ross Goroshin, Arjun Jain, Yann LeCun, and Christoph Bregler. Efficient object localization using convolutional networks. In *CVPR*, 2015. 2
- [56] Bishan Wang, Jingwei He, Lei Yu, Gui-Song Xia, and Wen Yang. Event enhanced high-quality image recovery. In *Computer Vision – ECCV 2020*, pages 155–171, Cham, 2020. Springer International Publishing. 1
- [57] Haoran Wang, Licheng Jiao, Shuyuan Yang, Lingling Li, and Zexin Wang. Simple and effective: Spatial rescaling for person reidentification. *IEEE Transactions on Neural Networks and Learning Systems*, 33:145–156, 2020. 6, 7
- [58] Taiqing Wang, Shaogang Gong, Xiatian Zhu, and Shengjin Wang. Person re-identification by video ranking. In *Computer Vision – ECCV 2014*, pages 688–703, Cham, 2014. Springer International Publishing. 6
- [59] Yingquan Wang, Pingping Zhang, Shang Gao, Xia Geng, Hu Lu, and Dong Wang. Pyramid spatial-temporal aggregation for video-based person re-identification. In *2021 IEEE/CVF International Conference on Computer Vision (ICCV)*, pages 12006–12015, 2021. 1, 2
- [60] Yingquan Wang, Pingping Zhang, Shang Gao, Xiaowei Geng, Huajie Lu, and Dong Wang. Pyramid spatial-temporal aggregation for video-based person re-identification. *2021 IEEE/CVF International Conference on Computer Vision (ICCV)*, pages 12006–12015, 2021. 6, 7
- [61] Zhikang Wang, Lihuo He, Xiaoguang Tu, Jian Zhao, Xinbo Gao, Shengmei Shen, and Jiashi Feng. Robust video-based person re-identification by hierarchical mining. *IEEE Transactions on Circuits and Systems for Video Technology*, 32(12):8179–8191, 2022. 3
- [62] David Weikersdorfer, Raoul Hoffmann, and Jörg Conradt. Simultaneous localization and mapping for event-based vision systems. In *International Conference on Virtual Storytelling*, 2013. 3
- [63] Fang Xu, Lei Yu, Bishan Wang, Wen Yang, Gui-Song Xia, Xu Jia, Zhendong Qiao, and Jianzhuang Liu. Motion deblurring with real events. In *2021 IEEE/CVF International Conference on Computer Vision (ICCV)*, pages 2563–2572, 2021. 3
- [64] Yichao Yan, Jie Qin, Jiabin Chen, Li Liu, Fan Zhu, Ying Tai, and Ling Shao. Learning multi-granular hypergraphs for video-based person re-identification. In *2020 IEEE/CVF Conference on Computer Vision and Pattern Recognition (CVPR)*, pages 2896–2905, 2020. 3
- [65] Fan Yang, Wei Li, Binbin Liang, and Jianwei Zhang. Spatiotemporal interaction transformer network for video-based person reidentification in internet of things. *IEEE Internet of Things Journal*, 10(14):12537–12547, 2023. 1
- [66] Xi Yang, Huanling Liu, Nannan Wang, and Xinbo Gao. Bidirectional modality information interaction for visible-infrared person re-identification. *Pattern Recognit.*, 161:111301, 2025. 1
- [67] Mang Ye, Zesen Wu, Cuiqun Chen, and Bo Du. Channel augmentation for visible-infrared re-identification. *IEEE Trans. Pattern Anal. Mach. Intell.*, 46(4):2299–2315, 2024. 1
- [68] Chenyang Yu, Xuehu Liu, Yingquan Wang, Pingping Zhang, and Huchuan Lu. Tf-clip: Learning text-free clip for video-based person re-identification. In *AAAI Conference on Artificial Intelligence*, 2023. 6
- [69] Shizhou Zhang, Wenlong Luo, De Cheng, Qin Yang, Lingyan Ran, Yinghui Xing, and Yanning Zhang. Cross-platform video person reid: A new benchmark dataset and adaptation approach. In *European Conference on Computer Vision*, 2024. 6
- [70] Tianyu Zhang, Longhui Wei, Lingxi Xie, Zijie Zhuang, Yongfei Zhang, Bo Li, and Qi Tian. Spatiotemporal transformer for video-based person re-identification. *ArXiv*, abs/2103.16469, 2021. 3

- [71] Zhizheng Zhang, Cuiling Lan, Wenjun Zeng, and Zhibo Chen. Multi-granularity reference-aided attentive feature aggregation for video-based person re-identification. In *2020 IEEE/CVF Conference on Computer Vision and Pattern Recognition (CVPR)*, pages 10404–10413, 2020. 3
- [72] Chong Zheng, Ping Wei, and Nanning Zheng. A duplex spatiotemporal filtering network for video-based person re-identification. In *2020 25th International Conference on Pattern Recognition (ICPR)*, pages 7551–7557, 2021. 1, 2
- [73] Liang Zheng, Zhi Bie, Yifan Sun, Jingdong Wang, Chi Su, Shengjin Wang, and Qi Tian. Mars: A video benchmark for large-scale person re-identification. In *Computer Vision – ECCV 2016*, pages 868–884, Cham, 2016. Springer International Publishing. 3, 6
- [74] Kaiyang Zhou, Yongxin Yang, Andrea Cavallaro, and Tao Xiang. Omni-scale feature learning for person re-identification. *2019 IEEE/CVF International Conference on Computer Vision (ICCV)*, pages 3701–3711, 2019. 6
- [75] Alex Zihao Zhu, Nikolay A. Atanasov, and Kostas Daniilidis. Event-based visual inertial odometry. *2017 IEEE Conference on Computer Vision and Pattern Recognition (CVPR)*, pages 5816–5824, 2017. 3
- [76] Yihao Zuo, Jiaqi Yang, Jiaben Chen, Xia Wang, Yifu Wang, and Laurent Kneip. Devo: Depth-event camera visual odometry in challenging conditions. *2022 International Conference on Robotics and Automation (ICRA)*, pages 2179–2185, 2022. 3
- [77] Dai Zuozhuo, Chen Mingqiang, Gu Xiaodong, Zhu Siyu, and Tan Ping. Batch dropblock network for person re-identification and beyond. In *IEEE International Conference on Computer Vision*, 2019. 2

## Supplementary Material

### A. Limitations and Future Work

Although S<sup>3</sup>CE-Net demonstrates strong performance, its reliance on spiking backbones introduces latency and hardware constraints. Additionally, our sampling strategy assumes consistent scene dynamics across sub-sequences, which may not hold for highly erratic pedestrian motion. Moreover, the lack of large-scale and realistic event-based Re-ID datasets limits the generalizability and scalability of current methods. Addressing these issues requires more adaptive or motion-aware modules and the construction of more comprehensive benchmarks, which we leave to future investigation.

### B. Dataset Details

The **PRID dataset** includes 385 and 749 person identities captured from two different camera viewpoints, with only the first 200 identities appearing in both non-overlapping cameras. This provides a foundation for cross-camera person re-identification. The **MARS dataset** is a large-scale and diverse dataset that includes 1,261 person identities and

20,008 video sequences, providing a comprehensive benchmark for video-based person re-identification. The **iLIDS-VID dataset** includes 300 person identities and 600 image sequences captured from two different camera viewpoints. This dataset is considered challenging due to factors such as similar clothing between different individuals, lighting and viewpoint variations across different camera perspectives, cluttered backgrounds, and random occlusions.

**Event-ReID (real-event dataset).** Event-ReID is the first publicly available *real* event-camera benchmark for person Re-ID. It was captured by four indoor Prophesee DVS cameras ( $640 \times 480$ ) and contains 33 identities walking across the four views, yielding 16 k annotated bounding boxes.

#### Pre-processing.

- (i) *Spatial cropping.* Each raw event stream is cropped to the pedestrian region using the hand+YOLO bounding box.
- (ii) *Fixed-time accumulation.* Events are integrated within a constant window  $\Delta t = 33.3$  ms ( $\sim 30$  fps), preserving polarity to form one voxel frame per window.
- (iii) *Long-sequence concatenation.* Consecutive, non-overlapping voxel frames from the same ID-camera tracklet are concatenated, producing clips of 3.4 s on average and up to 8 s ( $\sim 100$ –240 frames).
- (iv) *File organisation.* Each frame is stored as `IDxxx_cy_###.txt` under `output/IDxxx/cam_y/`; clips are indexed by consecutive numbers.

**Alternative setting.** To replicate a constant-event window, run the script with `--event.time=False` `--event.count=5000` ( $\sim 30$  fps); all other steps remain unchanged.

### C. Intra-Frame Relative Position Bias

To enhance intra-frame attention modeling in SSAM (Spike-guided Spatio-temporal Attention Mechanism), we introduce a learnable intra-frame relative position bias  $B$ , which captures spatial dependencies among tokens within a single event frame. Given an event tensor with  $N_s = H_s \times W_s$  tokens, each token  $i$  is assigned a 2D coordinate  $(h_i, w_i)$ . The relative position index between two tokens  $i$  and  $j$  is defined as:

$$\Delta_{ij} = (h_i - h_j, w_i - w_j) \quad (11)$$

Based on this, we construct a learnable relative position bias table  $P$  of size:

$$P \in R^{(2H_s-1) \times (2W_s-1)} \quad (12)$$

where each entry stores the bias corresponding to a specific spatial displacement. The final relative position bias matrix



is indexed as:

$$B_{i,j} = P[\text{relative\_index}(\Delta_{ij})], i, j \in \{1, 2, \dots, N_s\}, \quad (13)$$

where  $\text{relative\_index}(\Delta_{ij})$  is used to map spatial displacements to their corresponding entries in the relative position bias table  $P$ . The design is inspired by Swin Transformer [43].

## D. Spiking Neural Networks (SNNs)

As a third-generation neural network, Spiking Neural Networks (SNNs) differ from traditional neural networks in that they perform asynchronous computation, rather than processing all points globally. Additionally, the decay mechanism during the "firing" process allows SNNs to effectively handle temporal information. In this work, we adopt Leaky Integrate-and-Fire (LIF) neurons [2] to process the complex dynamic features in event data. The membrane potential update equation for the LIF neuron at layer  $l$  at time  $t$ :

$$V_l(t + \Delta t) = V_l(t) + \frac{\Delta t}{\tau_m} [-(V_l(t) - V_{rest}) + X_l(t)] \quad (14)$$

$V_l(t)$  is the membrane potential at the current time step  $t$ ,  $V_{rest}$  represents the resting potential,  $\tau_m$  is the membrane time constant, and  $X_l(t)$  represents the presynaptic input, which is computed as the weighted sum of the pre-synaptic inputs before the spike:

$$X_l(t) = \sum_{i=1}^n (w_i \sum_j \psi_i(t - t_j)) \quad (15)$$

$\psi_i(t - t_j)$  represents the  $i$ -th spike event that occurs at time  $t_j$ . During the forward propagation process, if  $V_l(t) > V_{th}$ , a spike is triggered, and the neuron sends a spike signal to the downstream neurons.  $V_{th}$  represents the membrane potential threshold. Voltage reset:

$$V(t) \rightarrow V_{reset} \quad (16)$$

When the membrane potential  $V_l(t) < V_{th}$ , the neuron will not fire a spike. The membrane potential  $V_l(t)$  gradually accumulates until it exceeds the threshold or continues to remain below the threshold.